https://doi.org/10.2352/ISSN.2470-1173.2018.09.IRIACV-278

Multi-view Surface Inspection Using a Rotating Table

***Tomoya Kaichi*†, *Shohei Mori*†, *Hideo Saito*†, *Junichi Sugano*‡, *Hideyuki Adachi*‡**
† ***Keio University, Kanagawa, Japan***
‡ ***Visco Technologies Corporation, Tokyo, Japan***

Abstract

In this paper, we introduce a method to visually inspect industrial parts by using multi-view images of an industrial part on a rotating table. During the visual inspection of the parts' surfaces, the relationship between the camera pose, the light vectors, and the normal vectors of a part's surface is the key factor in detecting abnormalities. We can change the relationship between the three factors by rotating the part; then, the abnormalities are visible in certain positional relationships. We, therefore, track the points on a part's surfaces in an image sequence and discriminate abnormal points (such as points on scratches or dents) from normal points based on pixel value transitions while rotating the part. The experimental results, which were based on real data of industrial parts, showed that the proposed method could detect the abnormalities on the surfaces.

Introduction

Various surface inspection methods for industrial parts, which apply image processing technology, have been created to detect abnormalities, such as scratches, dents, and discolorations [1–4]. Many of these methods inspect a part using a single image [1, 2]. However, it is sometimes difficult to detect abnormalities from one image (depending on the magnitude and position of the abnormalities). Figure 1 shows examples of enlarged images of scratches; (a) and (b), (c) and (d), and (e) and (f) are enlarged images of the same scratches on the test parts from different views. The scratches are visible in (a), (d), and (e) but invisible in the other images.

When a part is observed from many viewpoints, the relationship between the sight line vector, and light vectors, and the normal vectors of a part's surface changes. Then, abnormalities are visible in certain positional relationships as shown in Figure 1. Therefore, it is expected that inspection methods using multi-view images can effectively detect abnormalities. Armand *et al*. [5] proposed a method to detect defects using multiple images that are captured while the position of the light changes. This method detects minute scratches on the surface as well as the shape irregularities of the target object, which are difficult to detect with a single image. However, with this method, only a single surface can be inspected because the positional relationship between the target object and the camera is fixed.

We propose a surface inspection method that uses an image sequence that is taken while the part is rotated on a rotating table and while the lights and the camera are fixed. The proposed method tracks every point on the surfaces and compares the transitions of pixel values to detect abnormal points. To track the points on the surface of a part accurately, we propose two underlying methods: (1) a camera calibration method to estimate the positional relationship between the camera with a telecentric lens and the rotating table and (2) a pose estimation method for the rotating part. This method achieves the following three objectives.

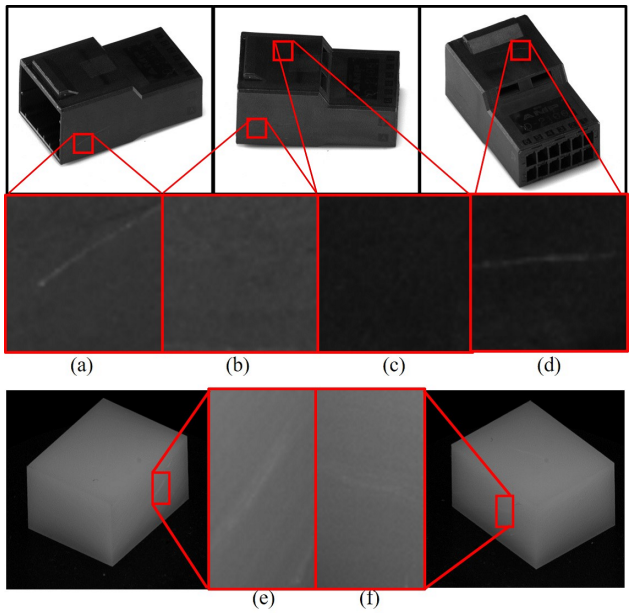

Figure 1. *Examples of scratches that are undetectable using a single image. (a) and (b), (c) and (d), and (e) and (f) are enlarged images of the same scratches from different views. The scratches are visible in (a), (d), and (e) but invisible in the other images.*

- Detecting fine abnormalities that are difficult to detect with a single image
- Inspecting the entire surface (except for the bottom of the surface)
- Inspecting without seeing sample parts in advance

The experimental results of using real data of industrial parts showed that the proposed method could detect and visualize abnormalities on surfaces. We verified that the proposed method could inspect the parts more accurately than a simple method that uses a single image.

Methods

System Overview

The proposed inspection method consists of two parts: tracking and discrimination procedures. In the tracking procedure, every point on the surface of the inspection target is tracked while the target is rotated on the rotating table to obtain the pixel value transitions of these points. The camera pose is calibrated and the pose of the inspection target is estimate so that we can track the

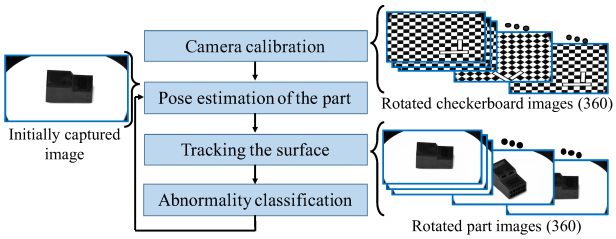

Figure 2. *System overview*

points on the target surfaces accurately. In the discrimination procedure, the points on abnormalities are discriminated based on the feature vectors made from the transitions. Figure 2 shows the overview of the proposed method as well as example images used for processing.

We assume that a camera with a telecentric lens is used to capture images in the proposed method. A camera with a telecentric lens is generally used for visual inspections, such as for scratch detection and size measurement of industrial products because the acquired image does not depend on the distance of the lens to the object. A robotic arm is used to place the part on a rotating table. Because industrial parts are produced based on CAD data, we assume that 3D CAD data of the part is given in advance.

Camera Calibration and Part Pose Estimation

We first estimate a positional relationship between a camera with a telecentric lens and a rotating table. The device configuration of the proposed method is shown in Figure 3. The camera parameters and camera pose can be calculated using an checkerboard image on the rotating table. Because a camera with a telecentric lens projects objects orthographically, the calibration can be performed using the method developed by Li *et al.* [6]. The camera parameters are composed of the magnification of the lens m and the pixel size in the u direction d_u and in the v direction d_v. The camera pose is represented by a 2×3 rotation matrix $\mathbf{R}$ and the translation vector $\mathbf{T}$. From the correspondence between the point in the world coordinate $\mathbf{P} = (X, Y, Z)$ and the projected point on the image $\mathbf{p} = (u, v)$, the projection matrix $\mathbf{M}$ can be obtained using Equation (1).

$$\begin{pmatrix} u \\ v \\ 1 \end{pmatrix} = \underbrace{\begin{pmatrix} m/d_u & 0 & 0 \\ 0 & m/d_v & 0 \\ 0 & 0 & 1 \end{pmatrix} \begin{pmatrix} r_{11} & r_{12} & r_{13} & t_x \\ r_{21} & r_{22} & r_{23} & t_y \\ 0 & 0 & 0 & 1 \end{pmatrix}}_{\mathbf{M}} \begin{pmatrix} X \\ Y \\ Z \\ 1 \end{pmatrix} \quad (1)$$

where r is an element of $\mathbf{R}$ and t_x, t_y are elements of $\mathbf{T}$.

In order to estimate the center of the rotating table, we track the corners of the checkerboard on the 360 images that are taken while rotating the table. The center of the ellipses, which are drawn by the trajectories of the corners, is the center of the rotating table in the image. The accurate positional relationship between the center of the rotating table and the camera can thus be obtained.

The initial pose of the part is estimated every time inspection starts. The part's pose is different each time because we assume that the part is put on the rotating table by a robotic arm. The pose is estimated based on the corners of the part in the image and

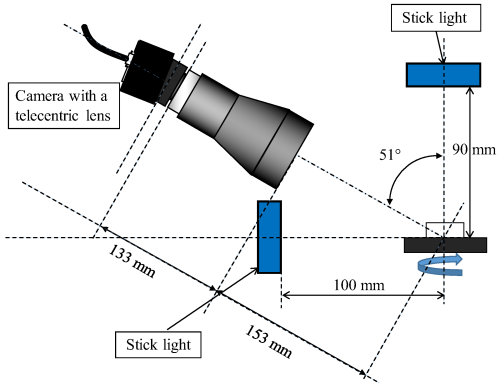

Figure 3. *Device configuration*

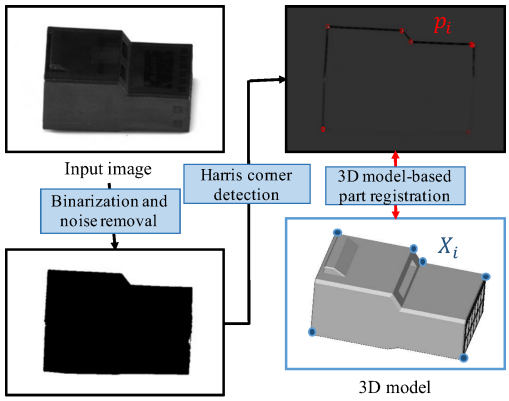

Figure 4. *Pose estimation of a part*

those of the 3D model as shown in Figure 4. In order to detect the corners, the image of the part is binarized, and the noise is removed using a dilation and erosion algorithm. We convert the denoised binarized image into a silhouette image through blob analysis. By detecting the corners [7] on the silhouetted image, we obtain the positions of the part's corners $\mathbf{p}_i$. $\mathbf{X}_i$ in Figure 4 represents the corners of a 3D model corresponding to $\mathbf{p}_i$, and $\mathbf{q}_i$ is the projected point of $\mathbf{X}_i$. By estimating x, y, and θ in Equation (3) to minimize the error function E in Equation (2), the position of the part can be estimated.

$$E(x, y, \theta) = \frac{1}{2} \sum_{i=1}^{N} (\mathbf{p}_i - \mathbf{q}_i)^2 \quad (2)$$

$$\tilde{\mathbf{q}}_i = \mathbf{M} \begin{pmatrix} \cos\theta & -\sin\theta & 0 & x \\ \sin\theta & \cos\theta & 0 & y \\ 0 & 0 & 1 & 0 \\ 0 & 0 & 0 & 1 \end{pmatrix} \tilde{\mathbf{X}}_i \quad (3)$$

where x and y represent the 2D position of the part on the rotating table, and θ is the rotation angle around the line perpendicular to the rotating table plane. $\mathbf{M}$ is the projection mrtrix expressed in Equation (1), and $\tilde{\mathbf{X}}_i$ represents the corners of the 3D model.

Abnormality Discrimination

The point on the surface is discriminated for whether it is abnormal based on the feature vector made from its pixel value transition. We design a feature vector that have the following two abilities:

- Robustness against the original color difference of one surface
- Applicability to a curved surface

When the images of the inspection target are captured every α degree while the target is rotated for 360°, the dimension of the pixel value transition of a certain surface $D = M/\alpha$. M is the number of images in which the surface is observed. The D dimensional raw data is smoothed by Gaussian filter, which is represented in Equation (4).

$$g_i(t) = \frac{1}{\sqrt{2\pi}\sigma} \exp(-\frac{f_i^2(t)}{2\sigma^2}) \tag{4}$$

where $f_i(t)$ is the transition of the pixel values at point i on the surface such that $g_i(t)$ after smoothing. Since images are taken every time the rotating table is rotated $\alpha°$, $g_i(t)$ is a discrete periodic function in which the cycle is D. The feature vector $\boldsymbol{x}_i$ is expressed by Equation (5) using $a_k(0 \leq k < D/2)$ and $b_k(1 \leq k < D/2)$, which are the coefficients obtained by a Fourier series expansion of $g_i(t)$.

$$\boldsymbol{x}_i = \{a_0^2, a_1^2 + b_1^2, a_2^2 + b_2^2, \cdots, a_{D/2-1}^2 + b_{D/2-1}^2\} \tag{5}$$

Note that the feature vector $\boldsymbol{x}_i$ does not depend on t. Therefore, the vector $\boldsymbol{x}_i$ has rotation angle invariance. We multiply a_k and b_k by their indices (i.e., $k \times a_k$, $k \times b_k$) to obtain color robustness.

The feature vectors are reduced through a principal component analysis [8]. When an Euclidean distance between a feature and the centroid of all features exceeds the threshold λ, the point that the feature represents is determined to be an abnormal point.

Experiments

First, we show the effectiveness of proposed calibration and part pose estimation methods. As a result of tracking procedure, the transitions of pixel values are presented in Figure 5. Next, we evaluate the accuracy of the proposed inspection method using real industrial parts comparing with single shot method. The relationship between the accuracy of the proposed method and threshold λ is evaluated using real parts with abnormalities.

Setup

We used a camera of 2048 × 1088 pixels (VTC-200CM-N) and a telecentric lens (MGTL014VM). The images captured in 2048 × 1088 pixels were resized into 1024 × 544 before they were used in the inspection process. In the experiments, we used the real industrial parts shown in Figure 4 as inspection targets. The maximum width, height, and depth of the part were 17.7mm, 14.5mm, and 30.7mm.

Surface Point Tracking

The camera calibration and the estimation of the position where the inspection target was placed were carried out using the method described in the *Camera Calibration and Part Pose Estimation* section. In order to investigate whether the optimization converged sufficiently within the assumed displacements, we checked the value of the error function E in Equation (2) when the initial value of (x, y, θ) changed. We confirmed that the error function E converged when the shift was within ± 20 mm with respect to x and y, and within ± 20° with respect to θ.

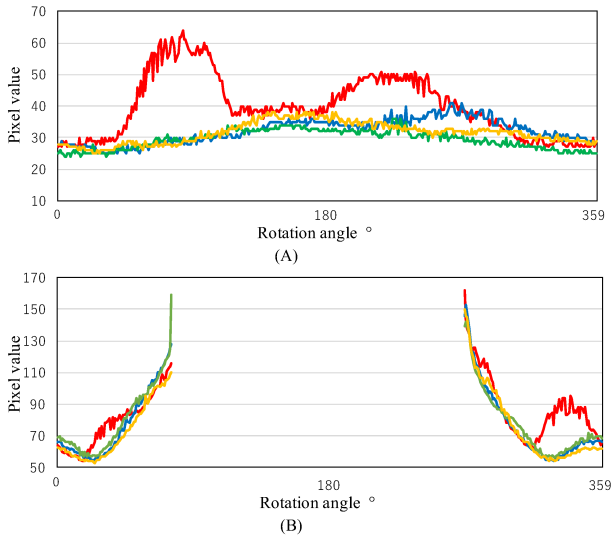

Figure 5. *Transitions of the pixel value: Graph (A) shows the pixel value transitions of the points on the top surface of the part. Graph (B) shows the points on the side surface. The red lines are the abnormal points on the scratches on the part's surface, while other lines are normal points around the abnormal points.*

Each surface was divided into grid points at 0.6 mm intervals, which was determined experimentally. In Figure 5, we plotted maximum pixel values in minimum lattices composed of these grid points. The graphs show the transitions of the pixel values while rotating the part and capturing every 1°. Figure 5 shows a clear difference between the red and the other plots, representing abnormal and normal points respectively.

Surface Abnormality Detection

We compared the proposed method with a single shot method for accuracy. The proposed method used all the images of the image sequence, whereas the single shot method used a single image in the image sequence. For the single shot method, we selected the input image from the image sequence where the abnormality was most clearly visible. The input image is binarized by an arbitrary threshold δ after edge detection with the Laplacian filter. Figure 6 shows the results of the proposed method whose threshold $\lambda = 1500$ and of the single shot method. The single shot method could not distinguish noise from an abnormality, as shown in Figure 6 (d), (e). We verified that the proposed inspection method, which used all the images of the image sequence was more robust to noise than the single shot method, which used each image individually.

Since the accuracy depends on the threshold λ, we observed the changes in the inspection accuracy depending on λ. The same shaped parts with scratches or dents were inspected at the setting of $\lambda = 1200$-1600. In Figure 7, the first two rows have scratch A and scratch B, and the third row has a dent on the surface. The part on the bottom of Figure 7 is a part without an abnormality. The

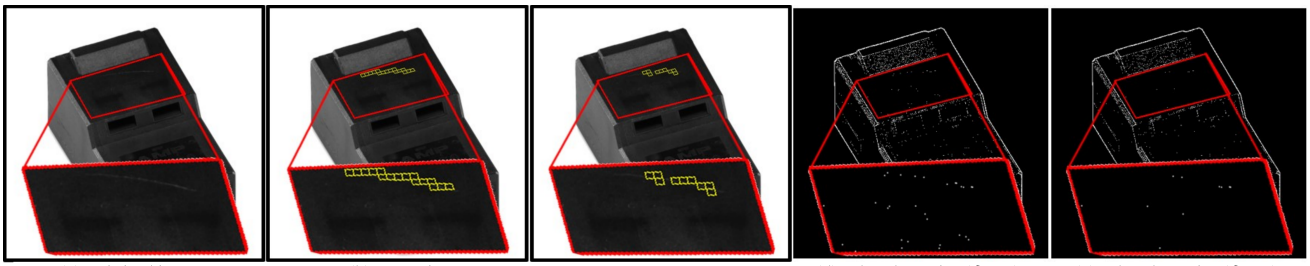

Figure 6. *Comparison between the proposed method and the single shot method*

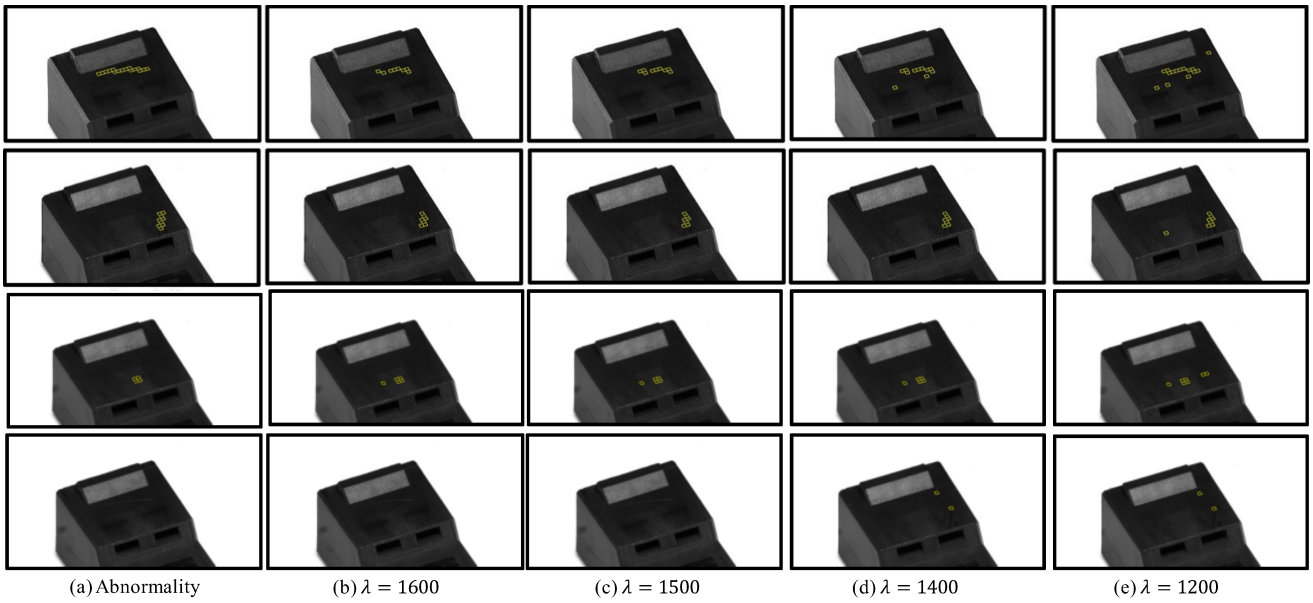

Figure 7. *Inspection results of the top surfaces by each threshold: the upper two parts have scratches, the third part has a dent, the bottom is the normal part without an abnormality*

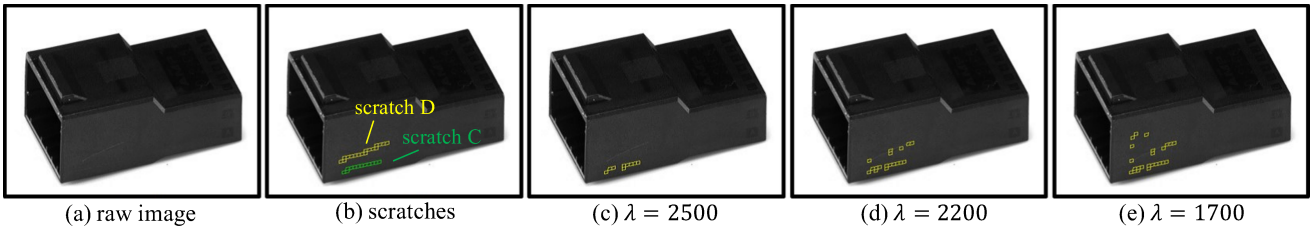

Figure 8. *Inspection results of the side surface*

Table 1: Relationship between the threshold and F-measure

Threshold λ	scratch A (%)	scratch B (%)	dent (%)
1600	66.7	87.5	88.9
1500	72.0	87.5	88.9
1400	66.7	87.5	88.9
1300	69.0	82.4	80.0
1200	71.0	82.4	72.7

average recall and precision when we inspected the three parts with abnormalities shown in Figure 7 are summarized in Table 1. The abnormalities were detected with a high accuracy when $\lambda = 1500$. In the experiments, the appropriate threshold λ was determined when the inspection surfaces were the same.

We inspected the side surface of the part. The surface had two scratches: scratch C was deep, which was easily visible when observed from cetain angles, and scratch D was a fine scratch compared to scratch C (Figure 8). When λ was set larger, as shown in Figure 8 (c), only the deep scratch was detected. The fine scratch was detected when λ became smaller (Figure 8 (d)). We confirmed that tolerance of abnormality could be set by adjusting the threshold λ.

Conclusion

In this paper, we proposed a surface inspection method that tracks the points on an industrial part's surfaces, examines each transition of the pixel values, and determines which points are abnormal points. We validated the proposed method using industrial parts, and we confirmed that the scratches and dent on the surface were detected. The future work includes tests using parts with various shapes and textures.

Acknowledgments

This research presentation is supported in part by a research assistantship of a Grant-in-Aid to the Program for Leading Graduate School for "Science for Development of Super Mature Society" from the Ministry of Education, Culture, Sport, Science, and Technology in Japan.

References

[1] T. S. Newman and A. K. Jain, "A survey of automated visual inspection", *Computer vision and image understanding*, Vol.61, No.2, pp.231-262, 1995.

[2] X. Xie, "A review of recent advances in surface defect detection using texture analysis techniques", *ELCVIA: electronic letters on computer vision and image analysis*, Vol.7, No.3, pp.1-22, 2008.

[3] F. Deng, Y. Ding, K. Peng, J. Xi, Y. Yin, and Z. Zhu, "Three-dimensional surface inspection for semiconductor components with fringe projection profilometry", Proc. SPIE 10023, pp.1-12, 2016.

[4] X. Xie and M. Mirmehdi, "TEXEMS: Texture exemplars for defect detection on random textured surfaces", *IEEE Transactions on Pattern Analysis and Machine Intelligence*, Vol.29, No.8, pp.1454-1464, 2007.

[5] Y. Armand, H. Saito, J. Sugano, and Y. Takizawa, "Detecting and measuring bent pins on electronic components", In SPIE Newsroom. 2009.

[6] D. Li and J. Tian, "An accurate calibration method for a camera with telecentric lenses", *Optics and Lasers in Engineering*, Vol.51, No.5, pp.538-541, 2013.

[7] C. Harris and M. Stephens, "A combined corner and edge detector", In Alvey vision conference. Vol.15, No.50, pp.10-5244, 1988.

[8] I. T. Jolliffe, "Principal Component Analysis and Factor Analysis", *Principal component analysis. Springer New York*, pp.115-128, 1986.

Author Biography

Tomoya Kaichi received his B.S. degree in engineering from Keio University, Japan, in 2016. He is currently in a master course at Keio University.

Junichi Sugano received his B.S. degree from Toho University, Japan, in 1995. He joined FAST Corporation in 1995, and engaged in vision library development. In 2008, he joined ViSCO Technologies Corporation and has engaged in research on image processing technology for cosmetic inspection applications.

Hideyuki Adachi received his B.S. degree in engineering from Osaka Electro-Communication University, Japan, in 1989. In 1989, he joined Analog Devices. He joined Cognex in 1996 and engaged in development of image processing technology and applications, and later served as Technical Application Manager. In 2003, he founded ViSCO Technologies Corporation and has served as CEO since then. He also worked on study and basic design of image processing algorithm as well as development of ViSCO products.

Shohei Mori received his B.S., M.S., and Ph.D. degrees in engineering from Ritsumeikan University, Japan, in 2011, 2013, and 2016, respectively. He was in JSPS Research Fellowship for Young Scientists (DC-1) until 2016. He is currently in JSPS Research Fellowship for Young Scientists (PD) at Keio University and a guest researcher at Graz University of Technology.

Hideo Saito received his Ph.D. degree in electrical engineering from Keio University, Japan, in 1992. Since then, he has been on the Faculty of Science and Technology, Keio University. From 1997 to 1999, he joined the Virtualized Reality Project in the Robotics Institute, Carnegie Mellon University as a visiting researcher. Since 2006, he has been a full professor in the Department of Information and Computer Science, Keio University.